Structural Insights into the Mechanism of PEPCK Catalysis[†,‡]

Todd Holyoak,*[,§] Sarah M. Sullivan,[§] and Thomas Nowak[||]

Department of Biochemistry and Molecular Biology, The University of Kansas Medical Center, Kansas City, Kansas 66160, and Department of Chemistry and Biochemistry, University of Notre Dame, Notre Dame, Indiana 46556

Received February 8, 2006; Revised Manuscript Received April 21, 2006

ABSTRACT: Phosphoenolpyruvate carboxykinase catalyzes the reversible decarboxylation of oxaloacetic acid with the concomitant transfer of the γ-phosphate of GTP to form PEP and GDP as the first committed step of gluconeogenesis and glyceroneogenesis. The three structures of the mitochondrial isoform of PEPCK reported are complexed with Mn^{2+}, Mn^{2+}−PEP, or Mn^{2+}−malonate−Mn^{2+}GDP and provide the first observations of the structure of the mitochondrial isoform and insight into the mechanism of catalysis mediated by this enzyme. The structures show the involvement of the hyper-reactive cysteine (C307) in the coordination of the active site Mn^{2+}. Upon formation of the PEPCK−Mn^{2+}−PEP or PEPCK−Mn^{2+}−malonate−Mn^{2+}GDP complexes, C307 coordination is lost as the P-loop in which it resides adopts a different conformation. The structures suggest that stabilization of the cysteine-coordinated metal geometry holds the enzyme as a catalytically incompetent metal complex and may represent a previously unappreciated mechanism of regulation. A third conformation of the mobile P-loop in the PEPCK−Mn^{2+}−malonate−Mn^{2+}GDP complex demonstrates the participation of a previously unrecognized, conserved serine residue (S305) in mediating phosphoryl transfer. The ordering of the mobile active site lid in the PEPCK−Mn^{2+}−malonate−Mn^{2+}GDP complex yields the first observation of this structural feature and provides additional insight into the mechanism of phosphoryl transfer.

Phosphoenolpyruvate carboxykinase [GTP/ITP:oxaloacetatecarboxylase (transphosphorylating, EC 4.1.1.32) (PEPCK)[1]] catalyzes the reversible decarboxylation of oxaloacetic acid with the concomitant transfer of the γ-phosphate of GTP (or ITP) to form PEP and GDP (IDP). PEPCK is a metal-requiring enzyme demonstrating an absolute requirement on divalent cations for activity (*2*). It has been demonstrated that Mn^{2+} is the best activator for chicken mPEPCK, with Co^{2+} and Mg^{2+} also providing activation but to a lesser extent (*2*). In addition to the enzyme-associated activating cation, a second divalent metal is required in the form of the metal−nucleotide substrate (*2*). The primary role of PEPCK in most organisms is the formation of PEP in the first committed step of gluconeogenesis and glyceroneogenesis. In mammals and higher eukaryotes, PEPCK activity is distributed among cytosolic and mitochondrial isozymes. The regulation of the cytosolic enzyme has been extensively studied, and it is found to be highly regulated at the level of transcription primarily through glucagon and insulin levels (*3*, *4*). In contrast, the mitochondrial isozyme, which represents 50% of the enzyme activity in adult human liver, is constitutively expressed (*3*). The mitochondrial and cytosolic isozymes from different species are highly homologous with levels of sequence identity of >60%. The protein studied herein is the mitochondrial isozyme isolated from chicken liver.

Two classes of PEPCKs exist in nature. The first, found in higher eukaryotic species such as mice, rats, chickens, and humans, utilizes GTP as the high-energy phosphoryl donor. An additional class of ATP-utilizing PEPCKs is found to exist in bacteria, C-4 plants, and yeast. While these enzymes share little sequence homology with the GTP class of enzymes, the structures of the active sites are reasonably conserved. It has therefore been proposed that an evolutionarily conserved mechanism of catalysis exists between the two classes with phosphoryl transfer occurring through an S_N2-like associative mechanism progressing through an enol−pyruvate intermediate (*5*−*11*).

Consistent with its role in gluconeogenesis, the importance of PEPCK in the maintenance of blood glucose levels during fasting in normal individuals and fasting hyperglycemia in non-insulin-dependent diabetes (NIDD) has been well documented (*12*, *13*). The therapeutic benefit of controlling flux through PEPCK has been shown in recent studies that demonstrate inhibition of PEPCK activity through the use of RNAi as an effective method of reducing fasting hyperglycemia in NIDD (*14*).

While a significant body of work detailing the mechanistic aspects [e.g., metal ion requirements (*15*), stereochemistry of carboxylation (*16*) and phosphoryl transfer (*11*), and pH

[†] This research was supported in part by NIH NCRR/COBRE 5 P20 RR16443-04 (T.H.).

[‡] Coordinates and structure factors have been deposited in the RCSB Protein Data Bank as entries 2FAF, 2FAG, and 2FAH.

* To whom correspondence should be addressed. Phone: (913) 588-0795. Fax: (913) 588-7440. E-mail: tholyoak@kumc.edu.

[§] The University of Kansas Medical Center.

[||] University of Notre Dame.

[1] Abbreviations: ASU, asymmetric unit; cPEPCK, cytosolic phosphoenolpyruvate carboxykinase; GDP, guanosine 5′-diphosphate; GTP, guanosine 5′-triphosphate; IDP, inosine 5′-diphosphate; ITP, inosine 5′-triphosphate; mPEPCK, mitochondrial phosphoenolpyruvate carboxykinase; NIDD, non-insulin-dependent diabetes; OAA, oxaloacetic acid; PEG, polyethylene glycol; PEP, phosphoenolpyruvate; PEPCK, phosphoenolpyruvate carboxykinase; PRR, water proton longitudinal relaxation rate; rmsd, root-mean-square deviation; TLS, translation/libration/screw.

10.1021/bi060269g CCC: $33.50
Published on Web 06/15/2006

dependence (*17*)] of PEPCK catalysis exists, the recent structure of the human cytosolic enzyme gave the first view of the structure of a GTP-dependent PEPCK (*18*). Despite this significant amount of information, several questions regarding the mechanism of PEPCK catalysis remain. In combination with the previous studies, the structural information reported here for the PEPCK−Mn^{2+}, PEPCK−Mn^{2+}−PEP, and PEPCK−Mn^{2+}GDP[2] complexes provides novel insights into the mechanism of the PEPCK-catalyzed reaction. In particular, the previously unappreciated role of two dynamic loop elements is shown. One of these mobile elements contains the hyper-reactive cysteine (C307) and the P-loop lysine (K309). The other mobile element comprises the active site lid, and the PEPCK−Mn^{2+}−malonate−Mn^{2+}-GDP structure provides the first observation of this element in the closed conformation.

MATERIALS AND METHODS

Materials. PEG 400 and 6000 were purchased from Fluka. GDP and PEP were obtained from Sigma. HEPES was purchased from Research Organics, and $MnCl_2$ was from Fisher. Malonic acid was purchased from Sigma, and a neutral saturated solution was prepared as previously described (*19*).

PEPCK Purification. Chicken liver PEPCK was purified as previously described (*20*). The concentration of PEPCK was determined using an extinction coefficient (ϵ_{280}) of 1.65 mg^{-1} mL^{-1} (*21*) and a molecular mass of 67 302 Da. The enzyme was shown to be >95% pure by SDS−PAGE. The enzyme utilized for these studies had a specific activity of 3.0−6.0 μmol of OAA formed min^{-1} mL^{-1} mg^{-1} (units per milligram) at 25 °C.

Crystallization. Initial crystallization conditions were determined by submission of PEPCK to the high-throughput crystal screening service at the Hauptman-Woodward Institute (Buffalo, NY) (http://www.hwi.buffalo.edu/ProductsServices/highthroughput/HighThroug.htm). Optimization of the initial crystallization conditions was performed by hanging-drop vapor diffusion utilizing kits from Hampton Research. Crystals of PEPCK used for data collection were grown by the hanging-drop method by mixing 2 μL of protein [containing 25 mg/mL PEPCK and 25 mM Tris (pH 8.0)] with 2 μL of mother liquor [0.1 M Hepes (pH 7.4) and 19% PEG 6000] and 0.5 μL of *n*-octanoylsucrose (Hampton Research). After crystallization, 0.5 μL of 1 M $MnCl_2$ was added to the crystallization drop. Crystals in complex with PEP were obtained by soaking the Mn^{2+}−PEPCK crystals in the presence of 4 mM PEP and 4 mM $MnCl_2$ overnight. Crystals of the PEPCK−Mn^{2+}−malonate−Mn^{2+}GDP complex were grown by the hanging-drop method using 4 μL of protein solution and 2 μL of mother liquor. Initial crystals were grown under the conditions indicated above with the addition of 0.5 μL of 20 mM GDP and 0.5 μL of 1 M $MnCl_2$ in the initial drops. These crystals were used to microseed drops set up as described above but utilizing 16% PEG 6000. The PEPCK−Mn^{2+} and PEPCK−Mn^{2+}−PEP crystals were cryoprotected by transferring the crystals to a 10 μL drop containing 21% PEG 6000, 0.1 M HEPES (pH 7.4), 20% PEG 400, and 4 mM $MnCl_2$. The PEPCK−Mn^{2+}−malonate−Mn^{2+}GDP crystals were cryoprotected by transferring the crystals sequentially to drops of 40, 50, and 60% saturated sodium malonate in a stepwise fashion (*19*). All crystals were cryocooled prior to data collection by immersion in liquid nitrogen.

Data Collection. Data were collected on cryocooled crystals of the PEPCK−Mn^{2+} and PEPCK−Mn^{2+}−PEP complexes kept at 100 K throughout data collection at SSRL beamline 11-1 using an ADSC Quantum-4 CCD detector. Data for the PEPCK−Mn^{2+}−malonate−Mn^{2+}GDP crystal kept at 100 K were collected using a RU-H3R rotating Cu anode X-ray generator with Blue Confocal Osmic mirrors and a Rigaku Raxis IV^{++} detector. All data were integrated and scaled with HKL-2000 (*22*).

Structure Determination and Refinement for PEPCK−Mn^{2+} and PEPCK−Mn^{2+}−PEP Structures. A homology model of mPEPCK was created using Swiss Model [http://swissmodel.expasy.org (*23*)]. The model was generated using the human cPEPCK structure [PDB entry 1KHG (*18*)] and the threaded sequence for chicken liver mPEPCK. The resulting model was used as the molecular replacement search model using MOLREP (*24*) in the CCP4 package (*25*). This molecular replacement solution was refined using Refmac5 (*26*) followed by manual model adjustment using COOT (*27*). Ligand, metal, and water addition and validation were also performed in COOT. A final round of TLS refinement was performed in Refmac5. In the PEPCK−Mn^{2+} and PEPCK−Mn^{2+}−PEP structures, a total of 20 TLS groups were utilized per chain, while in the PEPCK−Mn^{2+}−malonate−Mn^{2+}GDP structure, a total of 15 TLS groups were utilized. The groups were determined by submission of the PDB file to the TLSMD server [http://skuld.bmsc-.washington.edu/~tlsmd/index.html (*28*)]. PEPCK−Mn^{2+}−PEP crystals were isomorphous with the PEPCK−Mn^{2+} complex; therefore, the PEPCK−Mn^{2+} structure was used as the initial model for the refinement of the PEPCK−Mn^{2+}−PEP structure after the model was stripped of all water molecules, ligands, and ions. This initial model was subjected to a round of rigid body refinement in Refmac5 and refined in an identical fashion as described above for the PEPCK−Mn^{2+} structure. Phases for the triclinic PEPCK−Mn^{2+}−malonate−Mn^{2+}GDP complex were determined by molecular replacement using the PEPCK−Mn^{2+}−PEP structure as the starting model in CNS (*29*). The subsequent refinement process was identical to that of the PEPCK−Mn^{2+} and PEPCK−Mn^{2+}−PEP models. In addition, tight NCS constraints were applied during the initial rounds of refinement. In the final round of refinement, tight NCS restraints were retained, excluding those regions that were found to be outliers and were therefore excluded from the restraints. This approach was found to result in the lowest gap between R and R_{free}. The final data and model statistics for all structures are presented in Table 1.

Analysis with PROCHECK (*30*) demonstrates that all three models exhibit good stereochemistry with 89.4, 10.1, and 0.5% of the residues falling in the most favored, additionally allowed, and generously allowed regions of the Ramachandran plot, respectively, in the PEPCK−Mn^{2+} structure.

[2] Cryoprotection of the PEPCK−Mn^{2+}−Mn^{2+}GDP crystals with malonic acid results in a molecule of malonate binding at the active site and coordinating to the Mn^{2+} forming a PEPCK−Mn^{2+}−malonate−Mn^{2+}GDP complex. Since malonate is a weak competitive inhibitor against PEP (*1*), this complex may represent a mimic of the PEPCK−Mn^{2+}−PEP−Mn^{2+}GDP quaternary complex.

Table 1: Data and Model Statistics for the PEPCK−Mn^{2+}, PEPCK−Mn^{2+}−PEP, and PEPCK−Mn^{2+}−Malonate−Mn^{2+}GDP Structures

	PEPCK−Mn^{2+}	PEPCK−Mn^{2+}−PEP	PEPCK−Mn^{2+}−malonate−Mn^{2+}GDP
beam line	SSRL-11-1	SSRL-11-1	KUMC-rotating anode
wavelength (Å)	0.90	0.90	1.54
space group	$P2_1$	$P2_1$	$P1$
unit cell	$a = 110.8$ Å, $b = 47.7$ Å, $c = 127.2$ Å, $\alpha = \gamma = 90.0°$, $\beta = 111.3°$	$a = 110.4$ Å, $b = 48.0$ Å, $c = 126.3$ Å, $\alpha = \gamma = 90.0°$, $\beta = 111.4°$	$a = 74.6$ Å, $b = 90.9$ Å, $c = 103.3$ Å, $\alpha = 64.2°$, $\beta = 73.7°$, $\gamma = 71.2°$
resolution limit (Å)	34.1−1.7	35.1−1.9	32.8−2.1
no. of unique reflections	117687	90842	120981
completeness[a] (%; all data)	90.6 (83.3)	97.8 (93.8)	94.7 (84.3)
redundancy[a]	4.3 (3.9)	4.9 (4.5)	3.3 (3.0)
$I/\sigma_{(I)}$[a]	23.4 (2.7)	13.1 (2.4)	10.4 (1.9)
R_{merge}[a,b]	0.05 (0.50)	0.09 (0.54)	0.07 (0.48)
no. of ASU molecules	2	2	4
solvent content (%)	41	42	39
no. of amino acids residues	1194	1193	2432
no. of water molecules	995	879	1450
R_{free}[c] (%)	19.1	19.7	23.4
R_{work}[d] (%)	16.2	16.0	18.9
mean B value	24.9	13.5	16.2
Luzzati coordinate error (Å)	0.19	0.24	0.30
bond length rmsd (Å)	0.01	0.01	0.01
bond angle rmsd (deg)	1.34	1.55	1.31

[a] Values in parentheses represent statistics for data in the highest-resolution shells. The highest-resolution shell comprises data in the range of 1.76−1.70, 1.97−1.90, and 2.18−2.10 Å for the PEPCK−Mn^{2+}, PEPCK−Mn^{2+}−PEP, and PEPCK−Mn^{2+}−malonate−Mn^{2+}GDP data sets, respectively. [b] $R_{merge} = \sum|I_{obs} - I_{avg}|/\sum I_{obs}$. [c] $R_{work} = \sum||F_{obs}| - |F_{calc}||/\sum|F_{obs}|$. [d] See Brunger (*50*) for a description of R_{free}.

Similar values of 90.5, 9.1, and 0.3% and 89.0, 10.6, and 0.3% are observed in the PEPCK−Mn^{2+}−PEP and PEPCK−Mn^{2+}−malonate−Mn^{2+}GDP structures, respectively. In addition, one residue in the PEPCK−Mn^{2+}−malonate−Mn^{2+}-GDP structure is in the disallowed region of the Ramachandran plot (0.1%).

RESULTS AND DISCUSSION

Structural Details. mPEPCK crystallizes as a dimer in the asymmetric unit (ASU) in the PEPCK−Mn^{2+} and PEPCK−Mn^{2+}−PEP complexes, and four molecules are present in the PEPCK−Mn^{2+}−malonate−Mn^{2+}GDP ASU. These oligomers are crystallographic artifacts as the enzyme has been shown to be a functional monomer. Additional support for the artifactual nature of the observed oligomers comes from the observation that the dimerization is mediated by a molecule of *n*-octanoylsucrose that was found to be essential for crystallization of the PEPCK−Mn^{2+} complex (Figure 1). Several changes in the published amino acid sequence originally deduced from the sequencing of the mPEPCK gene (*31*) were observed (Figure S-1 of the Supporting Information). All but the addition of G129 and the change of S130 to proline were verified by resequencing of the original gene and by peptide mapping via Edman degradation and mass spectrometry (data not shown and ref *32*). The errors in the original gene sequence lie in GC rich regions, and the sequencing errors are most likely the result of compression in these areas. The highly GC rich nature of the gene is also a likely cause of the inability to recombinantly express the protein in bacterial or yeast systems (*32*). The changes in the primary sequence result in the mature enzyme being composed of 608 amino acids with a predicted molecular mass of 67 311 Da.

As would be expected with the high degree of sequence conservation between the human cytosolic and chicken mitochondrial enzymes, the overall fold of mPEPCK is identical to that of the previously determined structures of the human cytosolic isoform (*18*, *33*). An overall rmsd for C_α positions of 1.23 Å is observed when comparing the Mn^{2+} forms of the chicken mitochondrial and human cytosolic isozyme (PDB entry 1KHG). As previously noted, the enzyme represents a unique fold of the kinase family and to date is unique to the family of PEPCKs (*18*). The protein folds as a single domain with an N-terminal lobe and a C-terminal lobe forming an active site cleft between them as observed in the cPEPCK structures (*18*) (Figure 1). As in the structures of the complexes of human cPEPCK, no large domain movement occurs upon formation of the complexes containing nucleotide or PEP (*18*). This lack of domain movement is in contrast to what is seen for the ATP-utilizing PEPCKs that have been suggested to undergo domain movement upon formation of the nucleotide (*34*) and the PEP complexes (*35*).

The models are complete with the exception of amino acids 482−493, for which no density was visible in the PEPCK−Mn^{2+} and PEPCK−Mn^{2+}−PEP structures (Figure 2A). Consequently, these amino acids are missing from the final models of those structures. The equivalent loop is also absent in the human cPEPCK structures (*18*, *33*) and appears to be different from the lid observed in the *Anaerobiospirillum succiniciproducens* crystal structure (*36*). In the structure of the PEPCK−Mn^{2+}−malonate−Mn^{2+}GDP complex, this loop becomes ordered and closes tightly over the PEP binding site, thereby behaving like a lid that gates access to the active site (Figure 2B). The position of the lid clashes with the observed position of PEP in the PEPCK−Mn^{2+}−PEP structure with A486 lying only 1.54 Å from the phosphate of PEP in the superimposed structures (Figure 3A). The ordering of the lid upon nucleotide binding occludes access to the active site pocket that surrounds the bound Mn^{2+}, and the closed conformation seals the substrates in the quaternary complex of the enzyme (Figure 3). In the PEPCK−Mn^{2+}−malonate−Mn^{2+}GDP structure, the occupancies of the active site manganese ions and the metal−

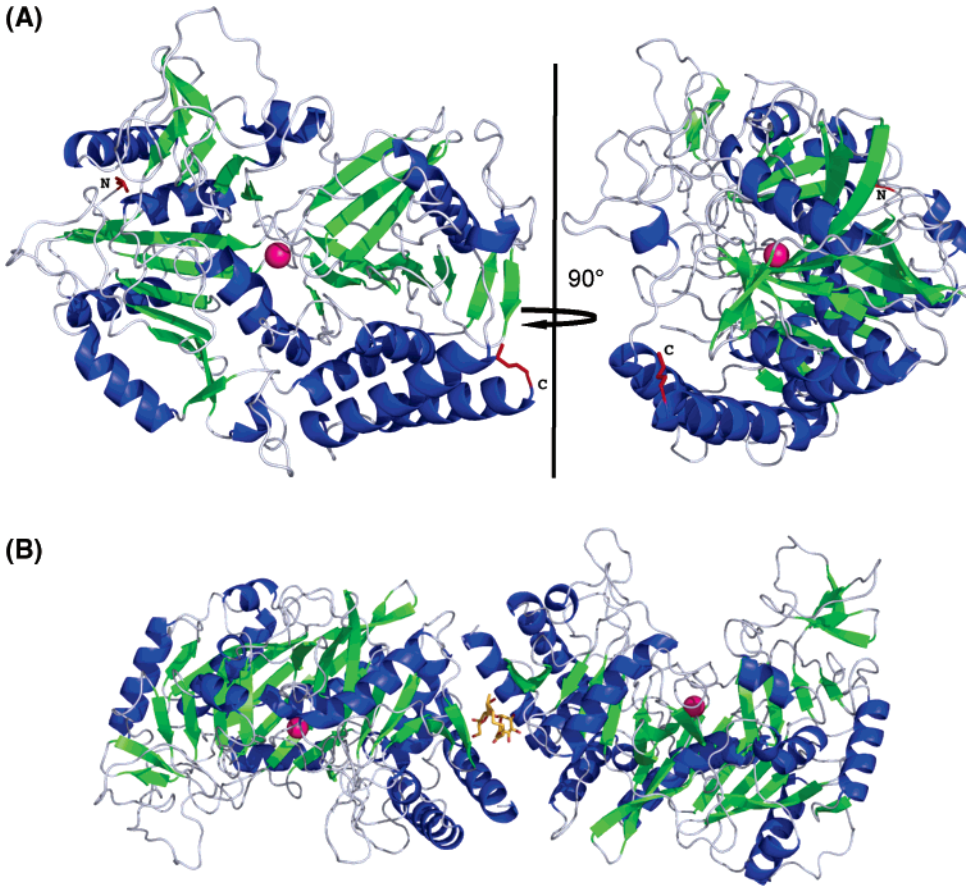

FIGURE 1: Overall structure of the mPEPCK (A) monomer and (B) crystallographic dimer. The active site is identified by the location of the Mn^{2+} which is rendered as a pink sphere. In panel A, the N- and C-termini are labeled and the N-terminal leucine and C-terminal methionine are rendered as red sticks. The molecule of *n*-octanoylsucrose that mediates the dimer interface is shown in panel B as a stick model. All figures were generated using Pymol (http://pymol.sourceforge.net/).

nucleotide manganese ions were found to be less than one. The occupancy of the metal ions in the four molecules in the ASU was manually adjusted so that the *B* factors for the Mn^{2+} were comparable to those of the coordinating ligands. This resulted in the disappearance of the negative difference density that was present when the occupancy for the ions was refined as one. This reduced occupancy is likely due to the chelating effect of the 3−4 M malonate solution that was used in cryoprotection of this crystal form. In molecules A, B, and D of the PEPCK−Mn^{2+}−malonate−Mn^{2+}GDP structure, a molecule of malonate is found coordinated to the active site Mn^{2+}. This is not surprising due to both the high concentration of malonic acid in the cryosolution and the ability of malonate to potentially mimic the putative enol−pyruvate intermediate (Figure 4C). Malonate has been shown to be a weak inhibitor against PEP (K_i > 50 mM) for mPEPCK (*1*). In molecule C, the density was consistent with a different orientation for the bound malonate where both carboxylate oxygens coordinate to the Mn^{2+} center.

A Functional Role for the Hyper-Reactive Cysteine. In the GTP-utilizing PEPCKs from rat cytosol and chicken mitochondria, as well as the ATP utilizing PEPCK from *Saccharomyces cerevisiae*, it has been observed that the modification of a single reactive cysteine residue results in inactivation of the enzyme (*37*−*42*). The identity of the reactive cysteine was shown in studies on rat cPEPCK to be C288 and the homologous C307 in chicken mPEPCK.[3] This cysteine residue is completely conserved in all PEPCKs. It was proposed that the protonation of this cysteine residue was necessary for optimal interaction of mPEPCK with IDP on the basis of pH−rate studies (*17*). The comparison of the PEPCK−Mn^{2+} structure to that of the PEPCK−Mn^{2+}−PEP and PEPCK−Mn^{2+}−malonate−Mn^{2+}GDP structures provides a mechanistic explanation for these observations. Unlike the human cytosolic structure, the predominant conformation of the P-loop in the mitochondrial PEPCK−Mn^{2+} structure results in the coordination of the hyper-reactive cysteine C307 to the active site Mn^{2+}, resulting in a tetrahedral geometry about the metal (Figure 4A). The additional metal ligands are identical to those in the human cPEPCK structure and are composed of the deprotonated side chains of K263, H283, and D330. The loop conformation adopted with cysteine coordinating to the metal presumably results in an inactive form of the enzyme as this loop position blocks the nucleotide-binding site (Figure 5). With the cysteine in a protonated state, the coordination to the Mn^{2+} is easily lost as demonstrated by the formation of the PEPCK−Mn^{2+}−PEP complex in situ through soaking of the PEPCK−Mn^{2+} crystals in a solution of PEP. There is evidence that the loop samples both the cysteine-coordinated conformation and the orientation found in the PEP-bound structure; in molecule A of the crystallographic dimer in the PEPCK−Mn^{2+} structure, a molecule of PEG 400 is located near the PEP binding site, and even though density for both P-loop conformations is present, the density was too poor to build a model for the cysteine-displaced conformation.

[3] K. C. Cheng and T. Nowak, unpublished observations.

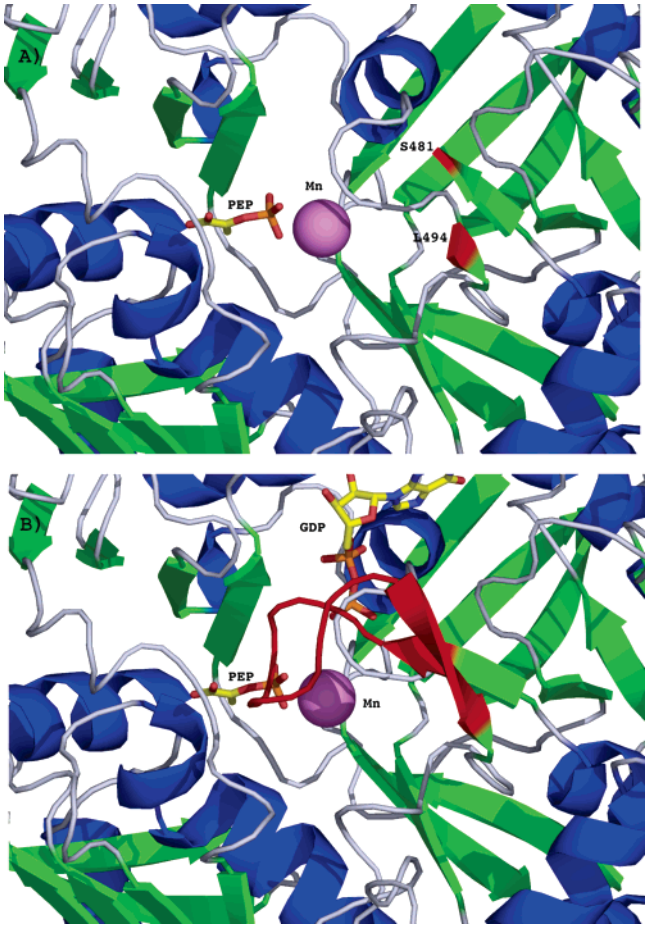

FIGURE 2: Ordering of the active site lid upon moving from (A) the PEPCK−Mn^{2+}−PEP complex to (B) the PEPCK−Mn^{2+}−malonate−Mn^{2+}GDP complex. In the ternary PEPCK−Mn^{2+}−PEP complex (A), density for residues 482−493 is not observed and the model is truncated at S481 and resumes at L494 (colored red). Upon formation of the PEPCK−Mn^{2+}−malonate−Mn^{2+}GDP complex, the loop (colored red) becomes ordered. The location of PEP in panel B was determined by superimposing the PEP and GDP structures.

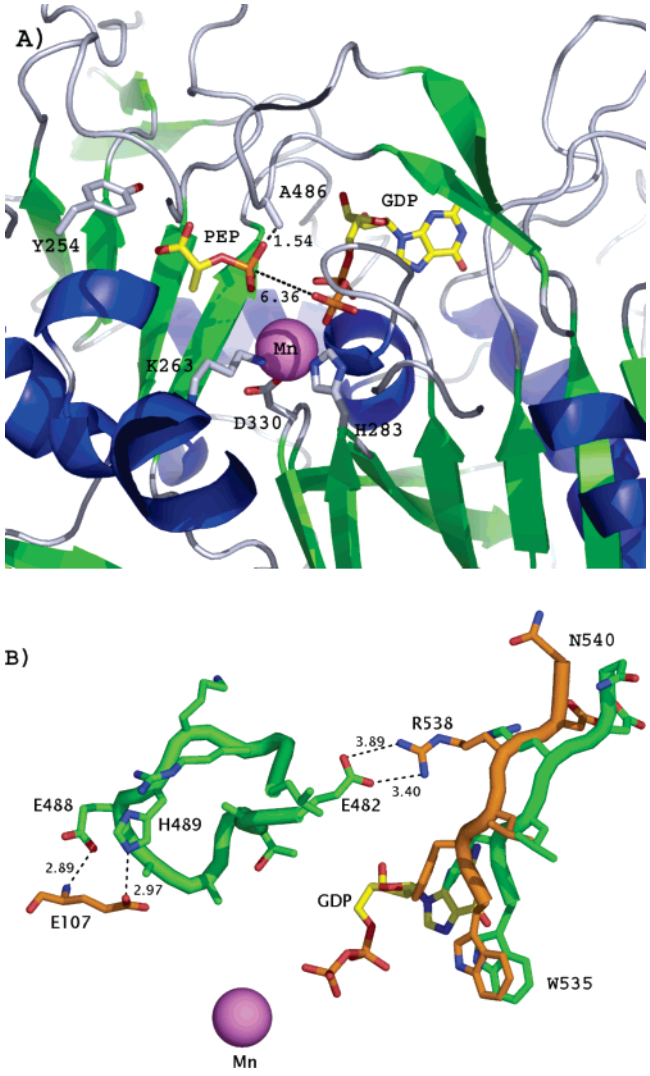

FIGURE 3: Ordering of the active site lid in the PEPCK−Mn^{2+}−malonate−Mn^{2+}GDP complex. (A) The distance between A486 of the closed lid and one of the oxygens of PEP is given. In addition, the distance between the phosphate of PEP and the β-phosphate of GDP in the pseudoquaternary complex is given. (B) Interactions of the lid with the nucleotide-binding region showing the displacement of the W535−N540 strand of the nucleotide-binding domain upon GDP binding that results in the formation of a salt bridge between R538 and E482. In addition, further stabilizing interactions between E107 and E488 and H489 of the active site lid are shown. The region from W535−N540 in the PEPCK−Mn^{2+}−PEP and PEPCK−Mn^{2+}−malonate−Mn^{2+}GDP structures is colored green and orange, respectively. All distances are in angstroms.

The observation of the cysteine-coordinated P-loop conformation provides structural evidence for the ionization of C307 appearing in the k_{cat}/K_M profile for IDP (*17*) since the deprotonation of the cysteine would be predicted to stabilize the C307 tetrahedral geometry, and to prevent nucleotide association (Figures 4A and 5). In addition to occluding the nucleotide-binding site, the C307-coordinated orientation of the P-loop does not allow for the correct positioning of the P-loop lysine (K309). K309 is poorly ordered in this complex (C_α *B* factor = 36.8). This is in contrast to its well-ordered position in the PEPCK−Mn^{2+}−PEP and PEPCK−Mn^{2+}−malonate−Mn^{2+}GDP complexes (C_α *B* factor = 19.7 and 14.6, respectively).

The involvement of C307 in coordinating to the active site metal in the holoenzyme complex provides a structural rationale for many previous peculiarities of PEPCK activity. Cation activation of PEPCK has been widely studied, with Mn^{2+} being the most efficient activator of the enzyme; however, Co^{2+} and Mg^{2+} can also substitute but with decreasingly less efficiency (*2*, *15*, *43*). While Zn^{2+} is able to partially activate the enzyme in the direction of PEP formation, no catalytic activity is observed in the direction of OAA formation (*2*). Since Zn^{2+} typically prefers sulfhydryl ligands, and tetrahedral geometry is a stable structure for Zn^{2+} coordination, we postulate that the observed loss of activity in the presence of Zn^{2+} is through stabilization of the C307-coordinated tetrahedral conformation. This observation also provides structural evidence for the observed stimulation of PEPCK activity by β-mercaptoethanol (*21*). In the absence of β-mercaptoethanol, it is possible that the inactive conformation of the P-loop is stabilized, resulting in the reduced level of turnover. The role of β-mercaptoethanol in the assay is not to keep the enzyme reduced (*39*). In in vitro studies, contaminant levels of Zn^{2+} inhibit mPEPCK activity and a lag is observed in the approach to the steady state. The presence of β-mercaptoethanol eliminates this lag (*39*). Since the corresponding cysteine and the P-loop in which it resides are completely conserved in all

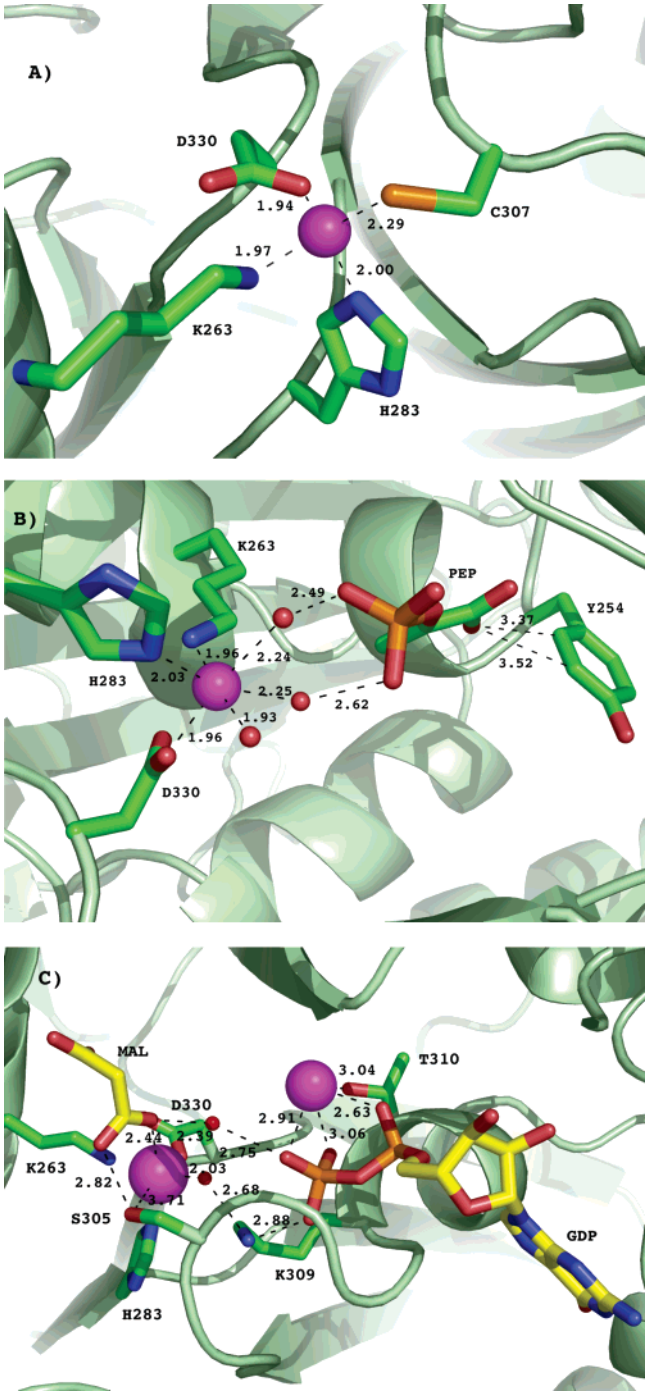

FIGURE 4: Coordination changes at the active site Mn^{2+} in progression from the (A) PEPCK−Mn^{2+} complex to the (B) PEPCK−Mn^{2+}−PEP and (C) PEPCK−Mn^{2+}−malonate−Mn^{2+}-GDP complexes. All distances are in angstroms. In panel C, the interactions between metal ligands K263, H283, and D330 have been omitted for clarity and are identical to the interactions shown in panel B. The manganese ions are rendered as pink spheres, while the relevant side chains, PEP, GDP, and malonate (MAL) are rendered as sticks. The water molecules are rendered as red spheres.

GTP-utilizing PEPCKs, it is reasonable to suggest that this regulation is somehow involved in the biological modulation of PEPCK activity. Consistent with these data is the observation that a more reduced environment results in a stimulation of gluconeogenesis in rat liver (*44*). The data therefore suggest that the opportunity for regulation of PEPCK activity may occur through the oxidative state, cation redistribution, and/or pH. In humans, this would allow for

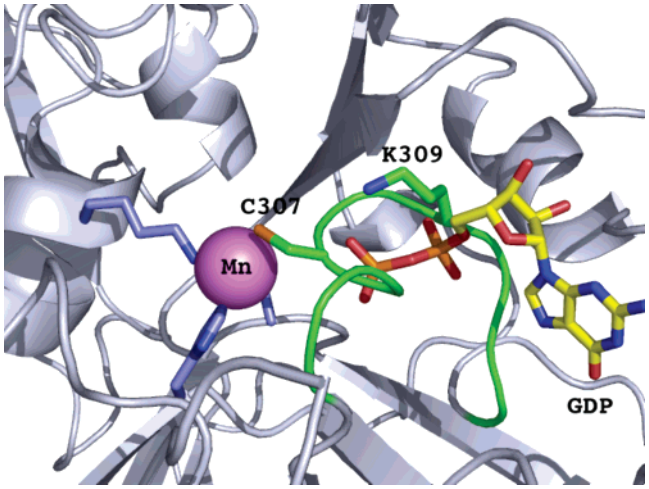

FIGURE 5: Steric conflict between the C307 P-loop orientation and GDP binding. The positions of the bound GDP nucleotide in the PEPCK−Mn^{2+}−malonate−Mn^{2+}GDP complex and the C307-coordinated P-loop conformation are mutually exclusive. The conformation of the P-loop that serves as part of the ligand structure of the bound Mn^{2+} that demonstrates tetrahedral coordination geometry in the PEPCK−Mn^{2+} structure is colored green. The C307 and K309 residues are rendered as sticks. The other metal ligands and the GDP are rendered as sticks and colored blue and yellow, respectively. The active site Mn^{2+} is rendered as a pink sphere.

control of gluconeogenic flux through mPEPCK that represents 50% of the enzyme activity in the adult liver. In addition, while cPEPCK is tightly regulated at the level of transcription, the enzyme has an estimated half-life of 6 h (*4*, *45*). Therefore, the C307-coordinated conformation could also provide a mechanism of immediate regulation of the cytosolic isoform.

Not only can the cysteine play an inhibitory and regulatory role, but also it is possible that the return of Mn^{2+} to the tetrahedral geometry also stimulates nucleotide product release. As previously mentioned, the PEPCK−Mn^{2+} structure suggests that the P-loop is dynamically sampling both orientations in the holoenzyme complex with the equilibrium in the crystal lying toward the tetrahedral coordination geometry. If this same equilibrium exists in solution, the thermodynamics would dictate a stimulation of product release due to the steric conflict between the conformation of the P-loop in the C307-coordinated state and the nucleotide-binding site.

Mechanism of Phosphoryl Transfer. Upon formation of the PEP complex, the active site Mn^{2+} adopts an octahedral geometry (Figure 4B) identical to that seen in the human cPEPCK structures and predicted by NMR and PRR studies (*15*). With the displacement of the cysteine residue from the coordination sphere of the active site Mn^{2+}, three water molecules coordinate to the ion, and the bound PEP coordinates in a second-sphere complex through the two equatorial waters. The carboxylate of PEP interacts in an edge-on fashion with the phenyl ring of Y254 with O1−CD2 and O1−CE2 distances of 3.37 and 3.52 Å, respectively (Figure 4B). This is similar to the molecule of PEP observed in the human cPEPCK−PEP structure (PDB entry 1KHF). The side chain of Y254 is observed to sample two conformations in the PEPCK−Mn^{2+}−malonate−Mn^{2+}GDP structure, one equivalent to the rearward orientation seen in the PEP-bound structure and the other resulting from a rotation of 7°

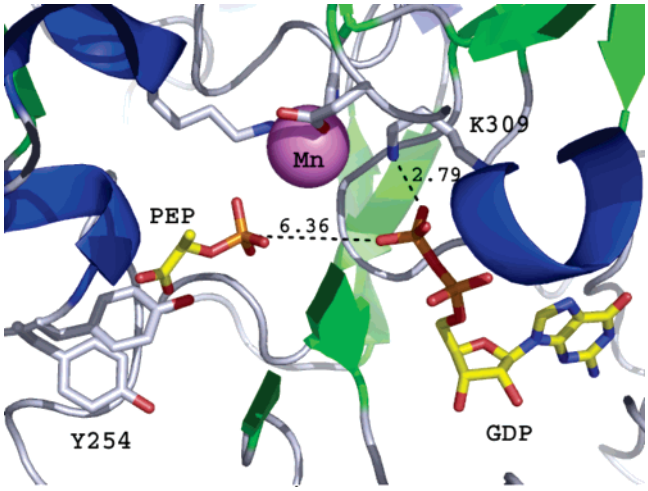

FIGURE 6: Pseudoquaternary PEPCK−Mn^{2+}−PEP−GDP complex. Superimposition of the PEPCK−Mn^{2+}−malonate−Mn^{2+}GDP complex with the PEPCK−Mn^{2+}−PEP complex results in the generation of a modeled quaternary complex. The distance between the phosphate of PEP and the oxygen of the β-phosphate of GDP is given. All distances are in angstroms. The two conformations of Y254 in the PEPCK−Mn^{2+}−malonate−Mn^{2+}GDP and PEPCK−Mn^{2+} structures are indicated, as is the bent orientation of the P-loop lysine (K309) that interacts with the β-phosphate of GDP.

about the $C_\alpha-C_\beta$ torsion (Figure 6). The involvement of Y254 in the interaction of PEP with the PEPCK−Mn^{2+} structure is consistent with the pH studies on k_{cat}/K_M for PEP that indicate the requirement for a residue with a pK_a of ~8 that is necessary for optimal interaction of PEP with the enzyme (*17*). As previously noted (*17*), deprotonation of Y254 would presumably stabilize the forward orientation of the Y254 side chain by strengthening the hydrogen bond between the phenolic oxygen of Y254 and the amide nitrogen of N422 (2.74 Å) and disfavoring the interaction between the backbone carbonyl of N422 and the phenolic oxygen (2.67 Å) of Y254 observed in the rearward orientation, thereby inhibiting the interaction of PEP with the enzyme.

The PEPCK−Mn^{2+}−malonate−Mn^{2+}GDP complex retains the six-coordinate Mn^{2+} center; however, two of the water molecules are displaced relative to the PEPCK−Mn^{2+}−PEP structure by the carboxylate of a molecule of malonate (2.44 Å) and a long interaction (3.71 Å) with the S305 hydroxyl (Figure 4C). The β-phosphate of GDP interacts with the active site Mn^{2+} in a second-sphere complex through the remaining water molecule (2.75 Å, Figure 4C). This distance is similar to the water−oxygen distance (2.5−2.6 Å) for the second-sphere PEPCK−Mn^{2+}−PEP interactions (Figures 4B). As previously mentioned, the formation of the PEPCK−Mn^{2+}−malonate−Mn^{2+}GDP complex results in the ordering of the mobile 482−493 lid in its closed conformation. The ordering of the active site lid seems to be initialized by a salt bridge between R538 and E482 (Figure 3B). π-Stacking interactions among the nucleotide base, F536, F544, and F549 in addition to the hydrogen bonds between R455 and O4′ (3.04 Å) of the ribose and N311 with one oxygen of the α-phosphate (2.62 Å) result in changes in the nucleotide-binding pocket that allow for a different orientation of R538 in the PEPCK−Mn^{2+}−malonate−Mn^{2+}GDP complex. This new orientation allows R538 to form a salt bridge with E482 that shifts the equilibrium position of the active site lid toward the closed position. This closed orientation is further stabilized through the interaction of H489 and E488 with the side chain and backbone amide of E107, respectively (Figure 3B). Since the position of E107 does not change upon formation of the PEPCK−Mn^{2+}−malonate−Mn^{2+}GDP complex, the interactions between E107 and lid residues H489 and E488 alone are apparently not sufficient to stabilize the closed conformation. Therefore, after formation of the stabilizing salt bridge, further stabilization of the closed conformation is imparted by the hydrogen bonds formed among E107, H489, and E488. It is interesting to note that while E107, E482, E488, and H489 are conserved in human, mouse, chicken, and rat isozymes, R538 is conserved only within the mitochondrial isozymes. The corresponding residue in the cytosolic isozymes is a conserved lysine residue. This raises the possibility that the arginine to lysine change, though conservative, would result in a weaker lysine−glutamate salt bridge. It is possible that this weaker interaction could change the behavior of the active site lid and may explain the suggested difference in kinetic mechanisms between the mitochondrial and cytosolic isozymes (*15*, *46*−*48*).

By this model, the closed conformation of the active site lid should result in the movement of PEP toward the active site Mn^{2+} and to the bound nucleotide in the quaternary complex as the side chain of A486 lies only 1.54 Å from the position occupied by the phosphate oxygen of PEP in the superimposed structures (Figure 3A). Further evidence for the displacement of PEP through the closure of the lid comes from the observation of a molecule of malonic acid bound in the PEP binding pocket in the PEPCK−Mn^{2+}−malonate−Mn^{2+}GDP complex (Figure 7). Unlike the molecule of PEP in the PEPCK−Mn^{2+}−PEP complex, the carboxylate of malonate coordinates directly to the Mn^{2+}, displacing two of the bound water molecules. This suggests that in a catalytically competent quaternary complex, the phosphate of PEP could be displaced from the location it occupies in the PEPCK−Mn^{2+}−PEP ternary complex and move toward the metal and interact by direct coordination to the Mn^{2+}, which previous NMR experiments suggested (*15*). In a concerted mechanism, the movement to inner-sphere coordination would presumably increase the electrophilic character of the PEP phosphate through greater polarization of the P−O bond, making it more susceptible to nucleophilic attack by the β-phosphate of GDP (*5*). Alternatively, if the reaction occurs in a stepwise fashion, malonate may be acting as a mimic of a potential enolate of pyruvate intermediate, and this intermediate would be stabilized by direct coordination to the metal center. From an analysis of the location of the bound malonate or the location of the phosphate of bound PEP, it is clear that the distance between either of the two ligands is too long for direct transfer of the phosphate to the nucleotide if the superimposed PEPCK−Mn^{2+}−PEP and PEPCK−Mn^{2+}−malonate−Mn^{2+}GDP structures represent a true quaternary complex. Some structural changes must occur upon formation of the catalytic PEPCK−Mn^{2+}−PEP−GDP complex. The observed motion of the Y254 side chain could act to "push" PEP toward Mn^{2+} and/or the nucleotide, resulting in either direct coordination of the phosphate or inner-sphere stabilization of the enolate intermediate, depending on the nature of the mechanism. The motion of Y254 returning to the forward orientation in the complex would reduce the distance

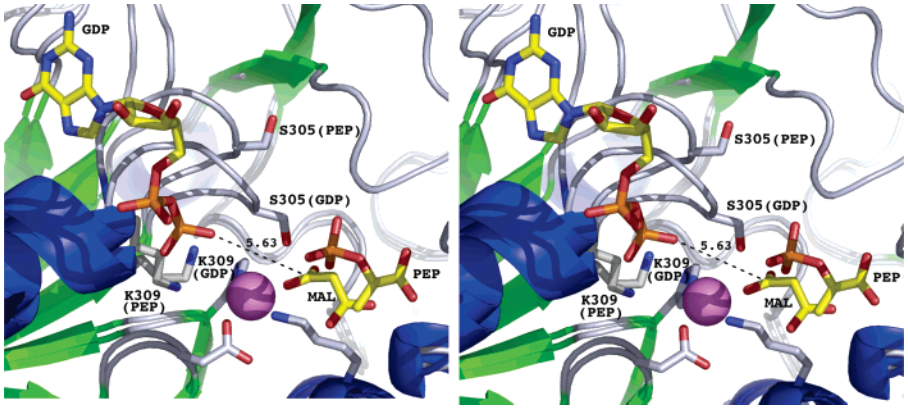

FIGURE 7: Stereoview showing the movement of the P-loop and the catalytic S305 progressing from the PEPCK−Mn^{2+}−PEP to the PEPCK−Mn^{2+}−malonate−Mn^{2+}GDP complex. Superimposition of the PEPCK−Mn^{2+}−PEP and PEPCK−Mn^{2+}−malonate−Mn^{2+}GDP structures illustrates the different orientations of the P-loop, K309, and S305 in these complexes. The distance between the carboxylate of malonate (MAL) and the β-phosphate of GDP is given in angstroms. PEP, malonate, GDP, S305, K309, and the active site Mn^{2+} ligands are shown as sticks, while the active site Mn^{2+} is rendered as a pink sphere.

for phosphate transfer in the PEPCK−Mn^{2+}−PEP−GDP complex as it progresses toward the transition state regardless of the nature of that transition state. Further constructive motions along the reaction coordinate would also be mediated through the closure of the active site lid as previously suggested.

In addition to these motions, the adoption of a third conformation of the mobile P-loop suggests the possibility that an additional mechanism is present. Upon formation of the GDP complex, the P-loop shifts and S305 adopts a conformation, placing it only 3.49 Å from the location of the phosphate of PEP in the PEPCK−Mn^{2+}−PEP structure and 2.82 Å from the carboxylate of the bound malonate (Figures 4 and 7). This third loop orientation is mediated by the movement of the P-loop lysine (K309) that shifts its C_α position by 2.1 Å when compared to its position in the PEP complex. This shift in position is the result of the adoption of a new side chain conformation of K309 that bends around to coordinate to the β-phosphate of GDP (Figure 7). The interaction of K309 in the mPEPCK−Mn^{2+}−malonate−Mn^{2+}GDP complex (Figure 4C) is different from that reported in the cPEPCK−β,γ-methylene−GTP structure and would explain why this conformation of the C307 loop was not observed in that complex of the cytosolic isozyme. This new conformation of the P-loop and the proximity of S305 to both the phosphate of PEP and the active site Mn^{2+} raise new questions about the mechanism of phosphoryl transfer mediated by PEPCK. One possible explanation for the new loop orientation is that it is an artifact of crystallization and mediated by the bound malonate. Evidence counter to this interpretation comes from the observation that the third conformation of the C307 loop is consistent with the observed protection of PEPCK from thiol modification in both rat cytosolic and chicken mitochondrial isoforms (*39*, *40*). Those studies demonstrated protection from modification such that the degree of protection is mediated in the following order: GDP > GTP ≫ PEP. The movement of the loop in the PEP, β,γ-methylene−GTP (human cPEPCK, PDB entry 1KHB), and GDP complexes of PEPCK shows the same correlation with respect to the degree of burial of the C307 side chain in the respective enzyme complexes (GDP > GTP ≫ PEP).

Because of the proximity of S305 to the phosphate of PEP, an attractive possibility for its role in phosphoryl transfer would be the involvement of a phosphoserine intermediate. The involvement of a phosphoserine intermediate, however, is not consistent with the observed inversion of configuration of the transferred phosphoryl group that was demonstrated to occur in chicken cPEPCK and mPEPCK (*10*, *11*) or the lack of kinetic evidence for a ping-pong mechanism. The kinetic results could be justified if the phosphoserine intermediate is very short-lived. An alternative hypothesis that is more consistent with the available kinetic, mutagenic, and structural data is based upon studies with the ATP-dependent PEPCK from *Escherichia coli*. In this enzyme, it has been proposed that phosphoryl transfer occurs through an associative mechanism (*5*, *7*). If the same mechanism occurs in the GTP-utilizing class of PEPCKs, it is possible that S305 could be functioning by forming a hexacoordinated activated phosphate during the phosphoryl transfer step. Recently, it has been shown that hexacoordinated phosphates exhibit greater reactivity than the traditional pentacoordinated species, and this increase in coordination geometry would lead to greater reactivity and in this instance allow the phosphate of PEP to be a better leaving group (*49*). Clearly, S305 plays an important role in the catalytic mechanism, and further study is needed to more precisely clarify that role.

In conclusion, our structural work has shown the existence of two previously unappreciated conformations for the active site P-loop. The first involves the coordination of the hyper-reactive C307 to the active site manganese ion, suggesting both a role in enzyme regulation through steric inhibition of nucleotide binding and a mechanism for stimulation of nucleotide product release. Second, the adoption of a third conformation of the P-loop suggests the involvement of S305 in the mechanism of phosphoryl transfer, possibly through the formation of a hexavalent phosphate species or the formation of a phosphoserine intermediate. Finally, the structure of the PEPCK−Mn^{2+}−malonate−Mn^{2+}GDP complex provides the first observation that the mobile active site lid appears to be involved in the mechanism of phosphoryl transfer. The motion of the active site lid and the intrinsic motion of Y254 suggest that these dynamic elements play a

role in pushing PEP toward inner-sphere coordination with Mn^{2+} and/or toward the bound nucleotide to facilitate catalysis.

ACKNOWLEDGMENT

The SSRL Structural Molecular Biology Program is supported by the Department of Energy, Office of Biological and Environmental Research, by the National Institutes of Health, National Center for Research Resources, Biomedical Technology Program, and by the National Institute of General Medical Sciences.

SUPPORTING INFORMATION AVAILABLE

Changes in the primary sequence of chicken mPEPCK suggested by the structural data and confirmed by primary sequence determination and mass spectrometry. This material is available free of charge via the Internet at http://pubs.acs.org.

REFERENCES

1. Guidinger, P. F., and Nowak, T. (1990) Analogs of oxalacetate as potential substrates for phosphoenolpyruvate carboxykinase, *Arch. Biochem. Biophys. 278*, 131−41.
2. Lee, M. H., Hebda, C. A., and Nowak, T. (1981) The role of cations in avian liver phosphoenolpyruvate carboxykinase catalysis. Activation and regulation, *J. Biol. Chem. 256*, 12793−801.
3. Croniger, C. M., Chakravarty, K., Olswang, Y., Cassuto, H., Reshef, L., and Hanson, R. W. (2002) Phosphoenolpyruvate carboxykinase revisited II. Control of PEPCK-C gene expression, *Biochem. Mol. Biol. Educ. 30*, 353−62.
4. Croniger, C. M., Olswang, Y., Reshef, L., Kalhan, S. C., Tilghman, S. M., and Hanson, R. W. (2002) Phosphoenolpyruvate carboxykinase revisited: Insights into its metabolic role. *Biochem. Mol. Biol. Educ. 30*, 14−20.
5. Delbaere, L. T. J., Sudom, A. M., Prasad, L., Leduc, Y., and Goldie, H. (2004) Structure/function studies of phosphoryl transfer by phosphoenolpyruvate carboxykinase, *Biochim. Biophys. Acta 1697*, 271−8.
6. Matte, A., Tari, L. W., Goldie, H., and Delbaere, L. T. (1997) Structure and mechanism of phosphoenolpyruvate carboxykinase, *J. Biol. Chem. 272*, 8105−8.
7. Sudom, A. M., Prasad, L., Goldie, H., and Delbaere, L. T. J. (2001) The phosphoryl-transfer mechanism of *Escherichia coli* phosphoenolpyruvate carboxykinase from the use of AlF3, *J. Mol. Biol. 314*, 83−92.
8. Tari, L. W., Matte, A., Goldie, H., and Delbaere, L. T. J. (1997) Mg^{2+}-Mn^{2+} clusters in enzyme-catalyzed phosphoryl-transfer reactions, *Nat. Struct. Biol. 4*, 990−4.
9. Chen, C. Y., Sato, Y., and Schramm, V. L. (1991) Isotope trapping and positional isotope exchange with rat and chicken liver phosphoenolpyruvate carboxykinases, *Biochemistry 30*, 4143−51.
10. Konopka, J. M., Lardy, H. A., and Frey, P. A. (1986) Stereochemical course of thiophosphoryl transfer catalyzed by cytosolic phosphoenolpyruvate carboxykinase, *Biochemistry 25*, 5571−5.
11. Sheu, K. F., Ho, H. T., Nolan, L. D., Markovitz, P., Richard, J. P., Utter, M. F., and Frey, P. A. (1984) Stereochemical course of thiophosphoryl group transfer catalyzed by mitochondrial phosphoenolpyruvate carboxykinase, *Biochemistry 23*, 1779−83.
12. Consoli, A., Nurjhan, N., Capani, F., and Gerich, J. (1989) Predominant Role of Gluconeogenesis in Increased Hepatic Glucose-Production in Niddm, *Diabetes 38*, 550−7.
13. Magnusson, I., Rothman, D. L., Katz, L. D., Shulman, R. G., and Shulman, G. I. (1992) Increased Rate of Gluconeogenesis in Type-Ii Diabetes-Mellitus: A C-13 Nuclear-Magnetic-Resonance Study, *J. Clin. Invest. 90*, 1323−7.
14. Gomez-Valades, A. G., Vidal-Alabro, A., Molas, M., Boada, J., Bermudez, J., Bartrons, R., and Perales, J. C. (2006) Overcoming Diabetes-Induced Hyperglycemia through Inhibition of Hepatic Phosphoenolpyruvate Carboxykinase (GTP) with RNAi, *Mol. Ther. 13*, 401.
15. Hebda, C. A., and Nowak, T. (1982) Phosphoenolpyruvate carboxykinase. Mn^{2+} and Mn^{2+} substrate complexes, *J. Biol. Chem. 257*, 5515−22.
16. Hwang, S. H., and Nowak, T. (1986) Stereochemistry of phosphoenolpyruvate carboxylation catalyzed by phosphoenolpyruvate carboxykinase, *Biochemistry 25*, 5590−5.
17. Holyoak, T., and Nowak, T. (2004) pH dependence of the reaction catalyzed by avian mitochondrial phosphoenolpyruvate carboxykinase, *Biochemistry 43*, 7054−65.
18. Dunten, P., Belunis, C., Crowther, R., Hollfelder, K., Kammlott, U., Levin, W., Michel, H., Ramsey, G. B., Swain, A., Weber, D., and Wertheimer, S. J. (2002) Crystal structure of human cytosolic phosphoenolpyruvate carboxykinase reveals a new GTP-binding site, *J. Mol. Biol. 316*, 257−64.
19. Holyoak, T., Fenn, T. D., Wilson, M. A., Moulin, A. G., Ringe, D., and Petsko, G. A. (2003) Malonate: A versatile cryoprotectant and stabilizing solution for salt-grown macromolecular crystals, *Acta Crystallogr. D59*, 2356−8.
20. Lee, M. H., and Nowak, T. (1984) Phosphorus-31 nuclear relaxation rate studies of the nucleotides on phosphoenolpyruvate carboxykinase, *Biochemistry 23*, 6506−13.
21. Hebda, C. A., and Nowak, T. (1982) The purification, characterization, and activation of phosphoenolpyruvate carboxykinase from chicken liver mitochondria, *J. Biol. Chem. 257*, 5503−14.
22. Otwinowski, Z., and Minor, W. (1997) Processing of X-ray Diffraction Data Collected in Oscillation Mode, in *Methods in Enzymology* (Carter, C. W., Jr., and Sweet, R. M., Eds.) pp 307−26, Academic Press, New York.
23. Schwede, T., Kopp, J., Guex, N., and Peitsch, M. C. (2003) SWISS-MODEL: An automated protein homology-modeling server, *Nucleic Acids Res. 31*, 3381−5.
24. Vagin, A., and Teplyakov, A. (1997) MOLREP: An automated program for molecular replacement, *J. Appl. Crystallogr. 30*, 1022−5.
25. Bailey, S. (1994) The Ccp4 Suite: Programs for Protein Crystallography, *Acta Crystallogr. D50*, 760−3.
26. Murshudov, G. N., Vagin, A. A., and Dodson, E. J. (1997) Refinement of macromolecular structures by the maximum-likelihood method, *Acta Crystallogr. D53*, 240−55.
27. Emsley, P., and Cowtan, K. (2004) Coot: Model-building tools for molecular graphics, *Acta Crystallogr. D60*, 2126−32.
28. Painter, J., and Merritt, E. A. (2005) A molecular viewer for the analysis of TLS rigid-body motion in macromolecules, *Acta Crystallogr. D61*, 465−71.
29. Brunger, A. T., Adams, P. D., Clore, G. M., DeLano, W. L., Gros, P., Grosse-Kunstleve, R. W., Jiang, J. S., Kuszewski, J., Nilges, M., Pannu, N. S., Read, R. J., Rice, L. M., Simonson, T., and Warren, G. L. (1998) Crystallography & NMR system: A new software suite for macromolecular structure determination, *Acta Crystallogr. D54* (Part 5), 905−21.
30. Laskowski, R. A., Macarthur, M. W., Moss, D. S., and Thornton, J. M. (1993) Procheck: A Program to Check the Stereochemical Quality of Protein Structures, *J. Appl. Crystallogr. 26*, 283−91.
31. Weldon, S. L., Rando, A., Matathias, A. S., Hod, Y., Kalonick, P. A., Savon, S., Cook, J. S., and Hanson, R. W. (1990) Mitochondrial phosphoenolpyruvate carboxykinase from the chicken. Comparison of the cDNA and protein sequences with the cytosolic isozyme, *J. Biol. Chem. 265*, 7308−17.
32. Holyoak, T. (2000) Kinetic, structural and genetic characterization of phosphoenolpyruvate carboxykinase, Ph.D. Thesis, University of Notre Dame, Notre Dame, IN.
33. Foley, L. H., Wang, P., Dunten, P., Ramsey, G., Gubler, M.-L., and Wertheimer, S. J. (2003) X-ray structures of two xanthine inhibitors bound to PEPCK and N-3 modifications of substituted 1,8-dibenzylxanthines, *Bioorg. Med. Chem. Lett. 13*, 3871.
34. Matte, A., Goldie, H., Sweet, R. M., and Delbaere, L. T. (1996) Crystal structure of *Escherichia coli* phosphoenolpyruvate carboxykinase: A new structural family with the P-loop nucleoside triphosphate hydrolase fold, *J. Mol. Biol. 256*, 126−43.
35. Encinas, M. V., Gonzalez-Nilo, F. D., Goldie, H., and Cardemil, E. (2002) Ligand interactions and protein conformational changes of phosphopyridoxyl-labeled *Escherichia coli* phosphoenolpyruvate carboxykinase determined by fluorescence spectroscopy, *Eur. J. Biochem. 269*, 4960−8.
36. Cotelesage, J. J. H., Prasad, L., Zeikus, J. G., Laivenieks, M., and Delbaere, L. T. J. (2005) Crystal structure of *Anaerobiospirillum succiniciproducens* PEP carboxykinase reveals an important active site loop, *Int. J. Biochem. Cell Biol. 37*, 1829.

37. Lewis, C. T., Haley, B. E., and Carlson, G. M. (1989) Formation of an intramolecular cystine disulfide during the reaction of 8-azidoguanosine 5′-triphosphate with cytosolic phosphoenolpyruvate carboxykinase (GTP) causes inactivation without photolabeling, *Biochemistry 28*, 9248−55.
38. Lewis, C. T., Seyer, J. M., and Carlson, G. M. (1992) Photochemical cross-linking of guanosine 5′-triphosphate to phosphoenolpyruvate carboxykinase (GTP), *Bioconjugate Chem. 3*, 160−6.
39. Makinen, A. L., and Nowak, T. (1989) A reactive cysteine in avian liver phosphoenolpyruvate carboxykinase, *J. Biol. Chem. 264*, 12148−57.
40. Lewis, C. T., Seyer, J. M., and Carlson, G. M. (1989) Cysteine 288: An essential hyperreactive thiol of cytosolic phosphoenolpyruvate carboxykinase (GTP), *J. Biol. Chem. 264*, 27−33.
41. Alvear, M., Encinas, M. V., Kemp, R. G., Latshaw, S. P., and Cardemil, E. (1992) ATP-dependent *Saccharomyces cerevisiae* phosphoenolpyruvate carboxykinase: Isolation and sequence of a peptide containing a highly reactive cysteine, *Biochim. Biophys. Acta 1119*, 35−8.
42. Encinas, M. V., Quinones, V., and Cardemil, E. (1990) *Saccharomyces cerevisiae* phosphoenolpyruvate carboxykinase: Physicochemical characteristics of the nucleotide binding site, as deduced from fluorescent spectroscopy measurements, *Biochemistry 29*, 4548−53.
43. Hlavaty, J. J., and Nowak, T. (1997) Formation and characterization of an active phosphoenolpyruvate carboxykinase-cobalt(III) complex, *Biochemistry 36*, 3389−403.
44. Arinze, I. J., Garber, A. J., and Hanson, R. W. (1973) The regulation of gluconeogenesis in mammalian liver. The role of mitochondrial phosphoenolpyruvate carboxykinase, *J. Biol. Chem. 248*, 2266−74.
45. Hopgood, M. F., Ballard, F. J., Reshef, L., and Hanson, R. W. (1973) Synthesis and degradation of phospoenolpyruvate carboxykinase in rat liver and adipose tissue, *Biochem. J. 134*, 445−53.
46. Felicioli, R. A., Barsacchi, R., and Ipata, P. L. (1970) Chicken liver mitochondrial phosphoenolpyruvate carboxykinase. Kinetic studies, *Eur. J. Biochem. 13*, 403−9.
47. Jomain-Baum, M., and Schramm, V. L. (1978) Kinetic mechanism of phosphoenolpyruvate carboxykinase (GTP) from rat liver cytosol. Product inhibition, isotope exchange at equilibrium, and partial reactions, *J. Biol. Chem. 253*, 3648−59.
48. Metchkarova, M. (2001) Kinetic mechanism of avian mitochondrial phosphoenolpyruvate carboxykinase, M.S. Thesis, University of Notre Dame, Notre Dame, IN.
49. Holmes, R. R. (2004) Phosphoryl transfer enzymes and hypervalent phosphorus chemistry, *Acc. Chem. Res. 37*, 746−53.
50. Brunger, A. T. (1992) Free R-Value: A Novel Statistical Quantity for Assessing the Accuracy of Crystal-Structures, *Nature 355*, 472−5.

BI060269G